Eur. Phys. J. D **36**, 339–351 (2005)
DOI: 10.1140/epjd/e2005-00281-7

THE EUROPEAN PHYSICAL JOURNAL D

Excitation dynamics of Rydberg states in C_{60}

M. Boyle[1], T. Laarmann[1], K. Hoffmann[1,a], M. Hedén[2], E.E.B. Campbell[2], C.P. Schulz[1,b], and I.V. Hertel[1,3]

[1] Max-Born-Institut, Max-Born Str. 2a, 12489 Berlin, Germany
[2] Dept. of Physics, Göteborg University, 41296 Göteborg, Sweden
[3] Free University of Berlin, Department of Physics, Arnimallee 14, 14195 Berlin, Germany

Received 23 March 2005 / Received in final form 29 July 2005
Published online 25 October 2005 –

Abstract. The electron and nuclear dynamics of C_{60} fullerenes irradiated with femtosecond laser pulses are investigated with photoelectron and photoion spectroscopy. The focus of this work is the detailed exploration of the population mechanism of Rydberg levels within the excitation process of neutral C_{60}. The effect of excitation wavelength, intensity, chirp, and polarization on the kinetic energy distribution of photoelectrons in single-pulse experiments gives first insight into the underlying processes. In combination with time-resolved two-color pump-probe spectroscopy depending on either pump, or probe pulse intensity, a more complete picture of the interaction can be drawn. The results point towards a very interesting but nevertheless complex behavior including four steps: (i) non-adiabatic multielectron excitation of the HOMO (h_u) → LUMO+1 (t_{1g}) transition; (ii) thermalization within the hot electron cloud on a time scale below 100 fs, followed by a coupling of energy to vibrational modes of the molecule via doorway state(s); (iii) population of electronically excited Rydberg states by multiphoton absorption, and (iv) single photon ionization from the excited Rydberg states. This excitation process results in a characteristic sequence of photoelectron lines in the photoemission spectra. The comparison of the experimental results with recent theoretical work gives convincing evidence that non-adiabatic multielectron dynamics (NMED) plays a key role for the understanding of the response of C_{60} to short-pulse laser radiation.

PACS. 36.40.-c Atomic and molecular clusters – 33.60.-q Photoelectron spectra – 33.80.Rv Multiphoton ionization and excitation to highly excited states (e.g., Rydberg states) – 61.48.+c Fullerenes and fullerene-related materials

1 Introduction

Optical control of molecular processes using intense femtosecond (fs) lasers is one of the hot topics in modern laser science [1]. One aims at manipulating potential energy surfaces to force the molecular system into specific reaction pathways. For instance, the possibility for selective bond dissociation and rearrangement in polyatomic molecules has recently been demonstrated [2]. This opens the door to new, exciting avenues in photochemistry with interesting potential applications in biology or medicine — keeping in mind that large molecules mediate fundamental processes in living organisms.

The feasibility of such experiments depends on a detailed knowledge of the fundamental processes initiated when focusing intense, short laser light pulses onto large finite molecules. In this context, the C_{60} fullerene can be regarded as an ideal model system for the investigation of strong-field phenomena in molecules with extended π electron systems. Due to the high symmetry, C_{60} with its 240 valence electrons can still be handled by theory [3,4] which in turn triggers detailed experimental studies and vice versa. The exploration of the electronic and nuclear dynamics in C_{60} has a long history. One astonishing early observation was the delayed ionization on a microsecond time scale upon irradiation with nanosecond laser pulses [5]. This has been explained by thermionic electron emission from vibrationally excited C_{60} fullerenes. Strong electron-phonon coupling leads to efficient heating of the nuclear motion during nanosecond laser excitation, and the subsequent ionization in turn is one important energy relaxation (cooling) channel [6]. It has been found that the ionization behavior depends sensitively on the excitation time scale, i.e. on the laser pulse duration τ [7]. The subject has recently been reviewed [8]. Hence we summarize here only some key aspects. For pulse durations above 1 ps one observes a characteristic bimodal fragmentation pattern of heavy fullerenes C_{60-2m} separated by C_2 units ranging down to $60-2m \gtrsim 32$ and a series of small carbon clusters C_n below $n \leq 28$. In contrast, for pulse durations below 500 fs the excitation energy tends to

[a] *Present address*: Department of Physics, University of Texas, Austin, Texas 78712, USA.
[b] e-mail: cps@mbi-berlin.de

remain in the electronic system (the electron-phonon coupling time being $\simeq 250$ fs), and multiply charged clusters are observed. Thermalization within the electronic system due to electron-electron scattering occurs on a time-scale of about 100 fs and ionization due to statistical electron emission after equilibration among the electronic degrees of freedom may be observed [9]. Direct multiphoton ionization dominates for very short laser pulses $\tau < 70$ fs [10]. As a fingerprint of the multiphoton process the photoelectron spectra of C_{60} exhibit a characteristic above threshold ionization (ATI) structure [7] in which the active electron absorbs more laser photons than necessary to overcome the ionization potential. This results in a kinetic energy distribution of photoelectrons, which exhibits a series of equally spaced maxima separated by the photon energy $h\nu$, as well known from atomic systems [11]. In addition, sharp peaks were discovered in the photoelectron spectra of C_{60} on top of the ATI series and the thermal electron contribution [12]. By solving the Schrödinger equation for a single active electron in a jellium-like potential [13], this structure could be clearly assigned to the population of several Rydberg series, which are then further ionized within the same laser pulse.

The observation of Rydberg peaks in the photoelectron spectra of C_{60} seems to be a clear signature of the "single active electron" (SAE) picture. Such quasi-static SAE description has been used traditionally to describe the ionization of atoms in strong laser fields [14–16]. It is bound to fail when dealing with large molecules exposed to intense laser pulses. This is particularly true for C_{60} with its large number of 60 delocalized π electrons. Recent theoretical investigation on laser-induced ultrafast dynamics in isolated C_{60} reveal that even at relatively low laser intensities on the order of 5×10^{10} W/cm^2 many ("active") electrons (MAE) are excited during a typical fs-laser pulse [3,4]. This points towards a more complex electronic and nuclear response of C_{60} exposed to strong laser fields which is governed by nonadiabatic multielectron dynamics (NMED) [17,18], as compared to the rather simple SAE approach.

In a recent note we communicated first results from a two-color pump-probe study, giving convincing evidence that the MAE/NMED picture is the key to understand the energetics and ultrafast dynamics of C_{60} in optical fs-laser fields, specifically the population mechanism of the Rydberg series [19]. Multielectron excitation comes into play through the t_{1g} electronic state (LUMO+1), which was identified as the doorway state to the excited state manifold. The important role of vibrational coupling to the initially excited state was verified by controlling the vibrational energy, respectively the temperature of the C_{60} fullerene. In the present paper we give a full account of this work, including additional experimental results, such as the effect of wavelength variation, intensity, polarization and positive, respectively negative chirp on the excitation dynamics of Rydberg states.

The paper is organized in the following way. In Section 2, we describe the experimental setup for the investigation of "hot" and "cold" fullerenes with single pulse or pump-probe photoelectron and photoion spectroscopy. In Section 3, the experimental data are presented. We first discuss the results obtained from single pulse experiments (Sect. 3.1). The second part focuses on results of two-color pump-probe spectroscopy (Sect. 3.2). This technique reveals detailed information on the ultrafast excitation dynamics, especially on nonadiabatic multielectron effects. In Section 3.3, photoelectron spectra of "hot" (770 K) and "cold" (80 K) C_{60} are presented. The comparison gives evidence for enhanced coupling of electronically excited states to nuclear vibrations in the hot system, i.e. the population of Rydberg states is affected by the phonon population density.

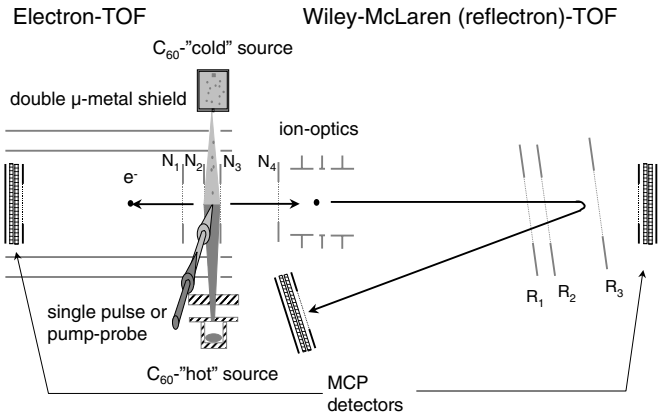

Fig. 1. Schematic of the experimental apparatus to record time-of-flight (TOF) photoelectron and photoion spectra of "hot" and "cold" C_{60} molecules upon laser irradiation. For details, see the text.

2 Experiment

Depending on the experimental requirements in terms of intensity, wavelength, spectral and temporal resolution, different laser sources were used for the measurements, all based on Ti:sapphire regenerative amplifier laser systems with 1 kHz repetition rate. An overview of the experimental setup is depicted in Figure 1. The Gaussian laser beams were focused onto the molecular beam produced either from heated gold grade C_{60} powder at a temperature of 770 K ("hot source") or in an aggregation cell, cooled by liquid nitrogen and using helium as the carrier gas. The "cold source" prepares molecules at a low temperature of approximately 80 K [20]. Special care was taken when using the cold source to avoid the production of $(C_{60})_n$ clusters by condensation of fullerene molecules. To this effect the temperature of the fullerene oven within the cold source and hence the C_{60} density in the gas phase was kept low enough so that no $(C_{60})_n^+$ ions were observed in the mass spectra.

The intensity of the laser beam in the focus was calibrated by a standard knife-edge method, as well as by using the known laser intensity dependence of multiphoton ionization of Xe atoms [21,22]. Both hot and cold fullerene beam source were mounted perpendicular to the

Table 1. Basic settings and distances of the time-of-flight (TOF) detector for ion detection.

region	distance [mm]	voltage applied [V]
N_2–N_3 (extraction)	20	2470–2085
N_3–N_4 (acceleration)	60	2085–0
N_4–R_1 (field-free drift)	1530	0
R_1–R_2 (brake path)	26	0–1670
R_2–R_3 (reflection)	234	1670–2800
R_1–MCP (field-free drift)	1086	0

laser beam path. The photoelectrons and ions generated at the intersection volume were detected using time-of-flight (TOF) spectrometers equipped with multi-channel plates (MCP) and counted using FAST multi-scalar cards. The ion detection axis is perpendicular to the laser and to the hot or cold C_{60} molecular beam, respectively. Unless specified explicitly in the text, the laser polarization vector was aligned parallel to the ion detection axis.

The positive ions are extracted with a static electric field. The ion optics in a reflectron Wiley-McLaren configuration assures time and spatial focusing. This results in a mass resolution of $m/\Delta m \simeq 2900$, hence enabling isotope identification in C_{60}. The basic settings and distances of the reflectron TOF are given in Table 1. Photoelectrons are detected without extraction field. They reach the detector in the direction opposite to the ion path through a field-free TOF drift tube of 450 mm length. The total distance between the laser focus and the electron MCP is 470 mm. The drift tube is double μ-metal shielded, in order to reduce the influence of stray magnetic fields on the flight path of the electrons. The inner surface is coated with graphite to avoid charging effects. The resolution of the electron TOF spectrometer ranges from 5 meV at a kinetic energy $E_{el} = 1$ eV to 400 meV at $E_{el} = 20$ eV. We mention that electrons with energies below 0.25 eV are not detected due to the temporal cutoff of the TOF and intensities slightly above that value cannot directly be compared with the remaining spectrum. We also note that with the present setup it is not possible to detect electrons and ions simultaneously. However, the apparatus allows fast switching between different detection modes and C_{60} molecular beam parameters, such as vibrational temperature, without breaking the vacuum. This assures almost identical excitation conditions in different measurements. Photoelectron and photoion spectra are averaged typically over 5000 to 20000 laser pulses using a standard PC programmed with LabVIEW.

3 Results and discussion

3.1 Single-pulse spectroscopy

Our experimental observations of pronounced sharp structures in the photoelectron spectra of C_{60} on top of the ATI-peaks and a broad thermal electron background [12] warrants further discussion. The structure is most clearly

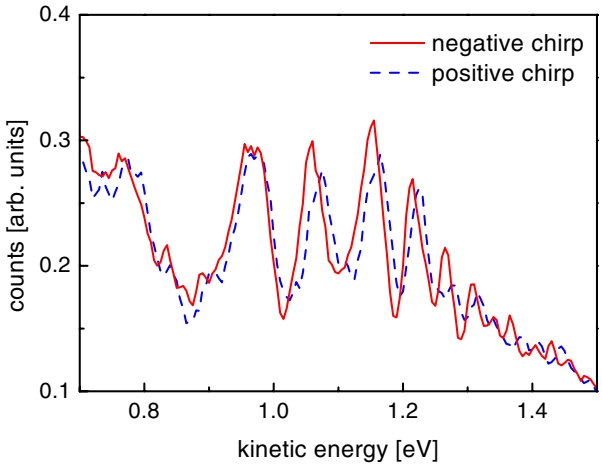

Fig. 2. Comparison of photoelectrons from C_{60} molecules irradiated with laser pulses at $\lambda = 800$ nm, a pulse duration of $\tau = 1.5$ ps, and a negative chirp (solid line: blue leads, red follows) or alternatively a positive chirp (dashed line: red leads, blue follows). The observed energy shift is on the order of the laser bandwidth $\Delta E = 10$ meV.

observed with a laser pulse duration of 1.5 ps at 800 nm wavelength with intensities on the order of 10^{12} W/cm^2. A typical example is shown in Figure 3a. Ionization from these electronically excited states occurs via single photon absorption within the same laser pulse. This leads to the characteristic sequence of distinct lines in the photoelectron spectra.

This interpretation is corroborated by an analysis of the photoelectron spectra obtained with different linearly chirped laser pulses. Figure 2 shows the effect of positively and negatively chirped pulses at 800 nm on the positions of several Rydberg peaks. The chirp was simply induced by detuning the compressor grating from its optimal position which, in addition, stretches the pulses from 180 fs to 1.5 ps. It is evident from Figure 2 that the position of the Rydberg peaks depends on the chirp while the intensity of the peaks is not affected. For negatively chirped pulses, where the red spectral components are delayed, the Rydberg peaks are shifted to lower kinetic energies as compared to the peak positions measured with positive chirped pulses, where the order of the spectral components is reversed. The observed shift of the peaks corresponds approximately to the laser bandwidth of $\Delta E = 10$ meV. This result can be explained if one assumes that the *excitation* of Rydberg states occurs mainly during the first part of the laser pulse while the *ionization* takes place towards the end of the pulse. This gives rise to the observed energy shift on the order of the laser bandwidth and justifies the assumption that the Rydberg states are excited and ionized during the same laser pulse.

A detailed analysis of the kinetic energy distribution of the photoelectrons in connection with a quantum mechanical calculation has allowed to identify the Rydberg levels excited [12]. The binding energies of the Rydberg states in C_{60} were derived by solving the radial Schrödinger equation for a single electron bound in a C_{60}^+ potential

Table 2. Experimental binding energies (in eV) and the effective principal quantum number n^* derived from the simple Rydberg formula $E = R/(n^*)^2$. Also shown is the assignment $n\ell$ resulting from the solution of the radial Schrödinger equation reproduced from reference [12]. The most right column gives the quantum defects δ as derived from the calculation.

exp. value	n^*	$n'\ell$ (nodes)	$n\ell$	calc. δ
1.01(5)	3.67(9)	$3h$	$8h$	4.46
0.88(8)	3.9(2)	$4g$	$8g$	4.00
0.76(5)	4.23(15)	$5d$	$7d$	2.96
0.73(2)	4.31(6)	?	?	
0.67(8)	4.5(3)	$5f$	$8f$	3.50
0.61(2)	4.72(8)	$6p$	$7p$	2.42
0.57(2)	4.88(9)	$4h$	$9h$	4.10
0.54(2)	5.01(10)	$6d$	$8d$	2.94
0.50(2)	5.22(10)	$3i, 5g$	$9i, 9g$	3.74
0.46(2)	5.43(12)	$6f$	$9f$	3.45
0.41(2)	5.76(15)	$2j$	$9j$	3.13
0.375(15)	6.02(12)	$5h$	$10h$	4.00
0.317(15)	6.55(16)	$7f$	$10f$	3.42
0.292(10)	6.82(12)	$3j$	$10j$	3.16
0.268(10)	7.12(14)	$6h$	$11h$	3.94
0.247(10)	7.42(15)	$8f$	$11f$	3.40
0.228(10)	7.72(18)	$4j$	$11j$	3.16
0.210(10)	8.0(2)	$7h$	$12h$	3.91
0.195(10)	8.3(2)	$6i, 8g$	$12i, 12g$	3.69
0.170(10)	8.9(3)	$8h$	$13h$	3.89
0.155(10)	9.3(3)	$7i, 9g$	$13i, 13g$	3.68
0.143(10)	9.7(4)	$6j, 10f$	$13j, 13f$	3.17
0.130(10)	10.2(4)	$9h$	$14h$	3.88
0.118(10)	10.7(5)	$7j, 11f$	$14j, 14f$	3.17
0.098(10)	11.7(7)	$8j, 12f$	$15j, 15f$	3.17
0.080(10)	13.0(9)	$12h$	$17h$	3.85
0.067(10)	14.2(12)	$13h$	$18h$	3.85

constructed from jellium-like potential [13] and a long-range Coulomb potential. As shown in reference [12], the calculated binding energies are in excellent agreement with the observed peaks in the kinetic energy distribution of photoelectrons. Table 2 shows a new compilation of these data. The effective principal quantum numbers n^* have been calculated by the simple Rydberg formula $E = R/(n^*)^2$ using the experimental binding energies obtained with 800 nm pulses. n^* ranges from 3.67 to 14.2. The integration of the one-dimensional radial Schrödinger equation allows one to assign the different Rydberg levels to a unique set of quantum numbers $n\ell$. While ℓ represents the angular momentum in the usual notation we have used in our previous publications [12,19] the number of nodes n' in the radial wave function to characterize the different orbits. From n' and ℓ one can easily derive the hydrogenic principal quantum number $n = n' + \ell$. We will use this notation ($n\ell$) throughout the remainder of the paper to label the different Rydberg states keeping in mind that the present experimental data do not allow an unambiguous assignment of the angular momentum. The last column of Table 2 gives the quantum defect δ derived from the calculated binding energies. Two observations are worth mentioning here. First, the quantum defect is almost constant for a series of $n\ell$ states with constant ℓ and large principal quantum numbers ($n > 10$). Second, in contrast to atoms the quantum defect does not decrease with increasing angular momentum. Instead, the h series ($\ell = 5$) has the largest quantum defect δ, while for higher and lower angular momentum states the value of δ is smaller. This non-atomic behaviour is clearly a consequence of the C_{60} being a hollow molecule. Although at first sight it appears quite surprising that this highly simplified model works so well, one easily verifies that once a Rydberg state is populated its characteristic radius is significantly larger than the fullerene radius of approximately 3.5 Å. Hence, the effective one particle treatment of the energetic problem is a very valid approximation. The peaks at respective energies in the photoelectron spectra are due to single-photon ionization from the initially excited Rydberg states whereas their population is most likely a collective multielectron effect as it will be discussed later in the text.

The final single photon ionization step in the excitation process is supported by studying details of the photoelectron spectra depending on the laser photon energy. Figure 3 (left side) shows the Rydberg photoelectron spectra for three different excitation wavelengths, (a) 800 nm, (b) 660 nm, and (c) 400 nm. The photoelectron spectra are plotted as a function of the electron binding energy $E_b(n\ell) = h\nu - E_{el}$ and can thus be compared directly. The assumption of single photon ionization of the Rydberg states is supported by the following arguments: (i) the kinetic energy of photoelectrons converges towards the respective photon energy, i.e. the accessible excited state for ionization is limited by the photon energy. (ii) The same Rydberg series are populated when using different excitation wavelengths, albeit with different intensity distributions. At first glance, this may seem to indicate a direct multiphoton excitation process of the Rydberg states with binding energies $E_b(n\ell)$. However, some important aspects warrant further discussion. Most critical is the energy mismatch between the observed excitation energy of the Rydberg states ($IP - E_b(n\ell)$) and a multiple of the photon energy: it is simply not possible to be in resonance with all observed Rydberg states simultaneously through the absorption of n photons with a given energy. The Fourier-limited energy bandwidth of the up to 2 ps long laser pulse is much too narrow to allow for the excitation of Rydberg states covering 1–2 eV in energy. Moreover, in this intensity regime the field-induced ponderomotive shift of the energy levels is also too small (<100 meV) to account for the observed energy mismatch. Thus, key mechanisms such as line broadening and energy sweeping, known from atomic systems in strong laser fields [24] cannot explain the Rydberg excitation process under the present conditions in C_{60} fullerenes.

Explaining this energy mismatch seems to be the key for a fundamental understanding of the excitation mechanism. Several possible scenarios can be envisioned. At first sight, one plausible explanation might be that the energy could be directly extracted from the high thermal energy content of C_{60} prepared in an effusive beam at a temperature of 770 K. About 5 eV are stored in the

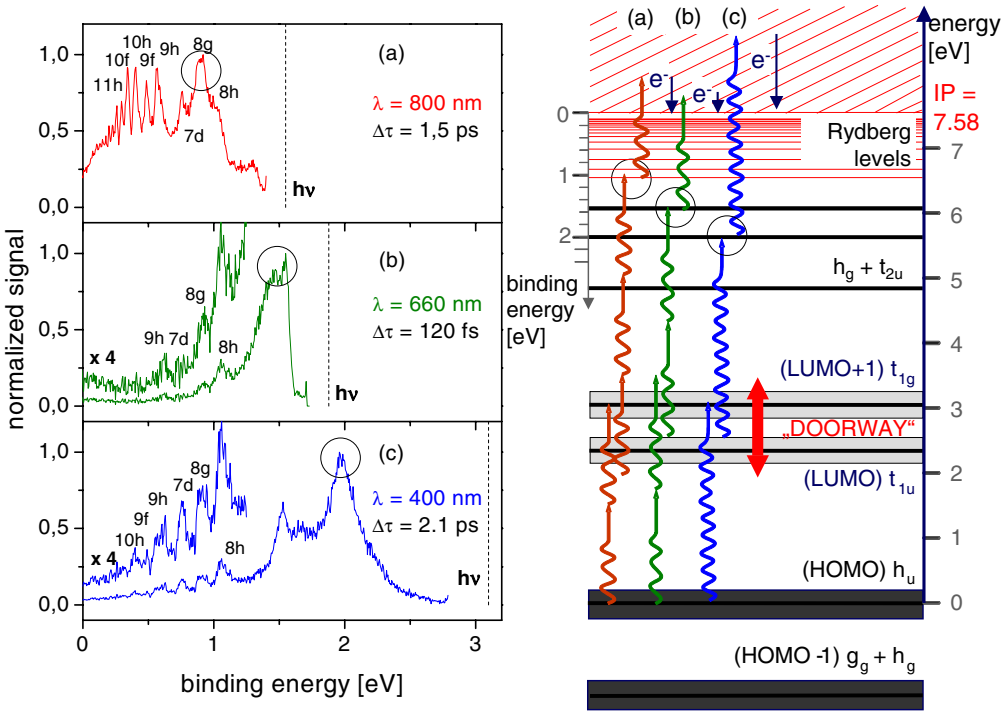

Fig. 3. Left: photoelectron spectra of C_{60} plotted versus the electron binding energy obtained for different laser parameters (a) 800 nm, 1.5 ps, 1.1×10^{12} W/cm^2, (b) 660 nm, 120 fs and (c) 400 nm, 2.1 ps, 3×10^{10} W/cm^2. The structures are assigned to several Rydberg series and lower lying excited states under the assumption that ionization occurs via single-photon absorption (for details, see the text); right: schematic orbital energy level diagram of C_{60} including the observed Rydberg states and some intermediate states [12,23], following the terminology applied in [4]. Shown are occupied HOMO and HOMO-1 levels (black boxes), unoccupied LUMO and LUMO+1 levels (shaded boxes), fast thermalization within the excited electrons and coupling to the nuclear vibrations (double arrow) to visualize non-adiabatic multielectron effects. Excitation processes for the different photon energies (a) to (c) with the highest transition probabilities (electron yield) are indicated (open circles).

$3n - 6 = 174$ vibrational modes. However, such concerted energy transfer from many nuclear degrees of freedom into the electronic system is very unlikely to happen in a direct multiphoton excitation process. Franck-Condon factors are expected to be prohibitive for such a mechanism, since the geometry of neutral C_{60} is very similar to that of singly charged C_{60}^+ to which the Rydberg states converge. Thus, one would expect a strong propensity for ionization without change of the nuclear geometry ($\Delta v = 0$), similar to that observed in one photon ionization [25]. As a consequence, the probability to excite the Rydberg state manifold directly from the molecular ground state is low, even taking nuclear vibrations into consideration. For understanding the spectroscopy of high lying Rydberg states in molecules, the inverse Born-Oppenheimer approximation [26] has to be evoked: in this approximation nuclear vibrations are considered to be fast compared to the orbiting time of the Rydberg electron and each vibrational degree of freedom "carries" its series of Rydberg levels. For the states of interest here we also have to consider that we may be in the intermediate region where the system cannot adequately be described by neither the Born-Oppenheimer nor the inverse Born-Oppenheimer approximation. This would lead to mixing of the electronic and vibrational states.

Another, more plausible explanation, under the high intensity excitation conditions of our experiment may be obtained by invoking excitation of intermediate electronic states during the laser pulse by single or multiphoton processes, followed by subsequent internal conversion (IC) processes or even transitions induced by the strong laser field itself through a "doorway state". Such processes have recently received great attention in the literature and a number of theoretical models have been discussed, including excitation from the ground state to an excited doorway state [27,28], nonadiabatic multielectron dynamics (NMED) [17,18], and time dependent potential energy crossings [29,30]. NMED has been used successfully to describe the dissociative ionization dynamics of different aromatic molecules as a function of their characteristic length and extension of the π-electron delocalization [17,18]. Using the results from time-of-flight mass spectroscopy and supported by numerical simulation, the authors have developed a model of the fs-laser interaction consisting of three key elements: (i) nonadiabatic excitation from the ground state to the excited-state quasi-continuum via a doorway state, (ii) dynamic polarization of the entire electronic system which leads to an exponential enhancement of this transition, and (iii) sequential energy deposition in the neutral molecule and the molecular ion before undergoing fragmentation. The concept of doorway electronic

states originate from the fact that the initial rate-limiting step in the excitation process can be regarded as a kind of bottleneck for the energy coupling into the electronic system.

Recent theoretical calculations on laser-induced ultrafast dynamics in isolated C_{60} using time-dependent density-functional theory (TDDFT) [3] and a matrix formalism [4] reveal that even at relatively low laser intensities of about 5×10^{10} W/cm^2 many electrons are excited ("active") during a typical fs-laser pulse (MAE). In a classical molecular picture one would typically invoke doubly excited states and internal conversion to describe such processes. Indeed, similar Rydberg structures have been reported for several organic molecules and the excitation mechanism has been explained there by such "superexcited" states [31,32]. In the context of the finite system C_{60} we consider MAE/NMED processes to be similar to Rydberg state excitation via such superexcited states. In the calculations by Zhang et al. [4], multielectron excitation of the LUMO+1 level of C_{60} is accompanied by strong vibrational excitation and massive energy exchange with the $a_g(1)$ breathing mode. Excitation of this mode has been reported for ultrafast excitation of undoped [33] and doped [34] thin films of C_{60}. However, in a strongly oscillating electric field one would intuitively expect the $h_u(1)$ prolate-oblate mode to be excited [35], rather than the totally symmetric $a_g(1)$ mode. Nevertheless, one may envisage this mode to become dominant if several electrons are excited into an antibonding electronic state in which electron repulsion would tend to inflate the fullerene. Interestingly, similar oscillations are found in rather sophisticated TDDFT calculations for fast collisional excitation of C_{60}, including also the nuclear motion of the system [36,37]. More recently, further simulations have shown that the modes excited in fs pulsed laser excitation depend strongly on pulse duration and intensity [38]. Although an experimental proof of such oscillating energy exchange of several eV between electronic and vibrational motion is still missing, the picture appears attractive to explain the observed non-resonant Rydberg excitation: the available "band" of electronic energies in the "doorway" state is broad enough to allow excitation of Rydberg states within an energetic range of 1–2 eV by e.g. 3 photons of 800 nm.

In order to illustrate the potential excitation processes for the different wavelengths studied, the right panel of Figure 3 reproduces the orbital energy diagram of the C_{60} fullerene, including the Rydberg states observed by Boyle et al. [12] and some other intermediate states [23] following the terminology applied in [4,8]. The diagram shows the occupied HOMO and HOMO-1 levels (black boxes), and the unoccupied LUMO and LUMO+1 levels (shaded boxes). The heavy double arrows indicate the fast thermalization within the excited electrons and the coupling of electronic and nuclear motion due to NMED. However, the reader should be warned that such a diagram necessarily indicates single electron orbital energies while the dynamics involves many active electrons — at least for the initial excitation step through the doorway state. Three scenarios, (a), (b), and (c), for Rydberg state excitation are indicated with 800, 660, and 400 nm photons, respectively. As seen, the LUMO+1 (t_{1g}) level is 2-photon (1-photon) resonant with 800 (400) nm excitation. Hence, we suggest it to be the "doorway state". In a strong 800 nm laser field its excitation is possible, as shown a in TDDFT calculation by Bauer et al. [39]. The calculation shows a strong second harmonic component of the dipole response when exciting C_{60} with a 26 fs 800 nm pulse at 3×10^{13} W/cm^2. In addition to this already broad response, which originates from electron-electron coupling, the interaction with the nuclear motion (which is not included in this particular TDDFT calculation) may lead to an further broadening of the excited levels and to field induced non-adiabatic coupling with other excited levels (e.g. with the LUMO (t_u)), as indicated by the heavy double arrows in the energy diagram in Figure 3 (right). This may eventually lead also to internal conversion with an irreversible exchange of energy between electronic and vibrational motion. The three scenarios are set such that they refer to the strongest peak in the experimentally observed Rydberg spectra. Scenario (a) illustrates how we can picture the excitation of the $8g$ Rydberg state from the populated doorway state(s) by three (possibly two) red photons. It is clear that in this scenario excitation up to the $11h$ state with three red photons should not be much less likely if we assume both the LUMO and the LUMO+1 to be excited in the initial step. This corresponds to the experimental observation. Scenario (b) and (c) indicate how the lower lying excited states with a binding energy of 1.5 eV and 2.0 eV are efficiently excited by two photons of 660 and one photon of 400 nm, respectively. This assignment is supported by the line-widths of these peaks, which are significantly broader (FWHM: 200–300 meV) than those of the "non-resonant" Rydberg lines (FWHM: <140 meV depending on the photon energy and quantum numbers). This can be understood in terms of a partial failure of the inverse Born-Oppenheimer picture for the lower lying Rydberg states due to the stronger interaction of the electron orbital with the C_{60}^+ ion core and, thus, resulting in a broader photoelectron peak. From scenario (b) and (c) it is also evident that two 660 nm photons or one 400 nm photon cannot reach the higher Rydberg levels from the LUMO+1 (in contrast to three red photons in scenario (a)). Hence the intensity in these cases rapidly decreases with increasing quantum numbers. In all three cases one additional photon finally ionizes the system and the corresponding kinetic energy of the photoelectron can be detected (downwards pointing arrows labeled e^-).

The alignment of the laser polarization vector with respect to the detector axis also affects the measured photoelectron yield. In Figure 4a the spectrum recorded with parallel polarization is compared to that recorded with perpendicular polarization. Photoemission from the Rydberg states indicated by arrows is significantly enhanced when the laser polarization axis points towards the detector. This again indicates that ionization occurs directly within one laser pulse. The high angular momenta involved in the processes lead to a significant anisotropy. Interestingly, the smooth background is less influenced by

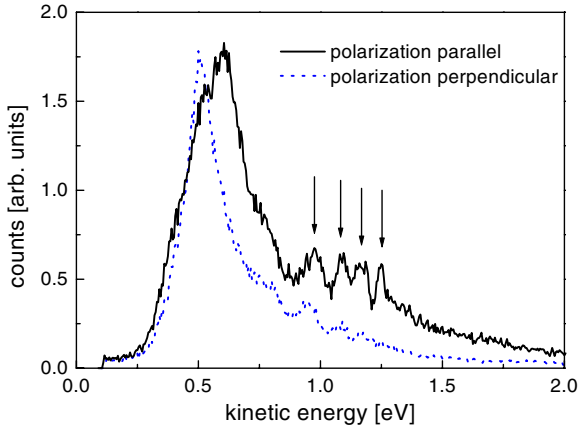

Fig. 4. Comparison of C_{60} photoelectrons recorded with the laser polarization vector oriented perpendicular (dotted line) and parallel (solid line) to the spectrometer axis.

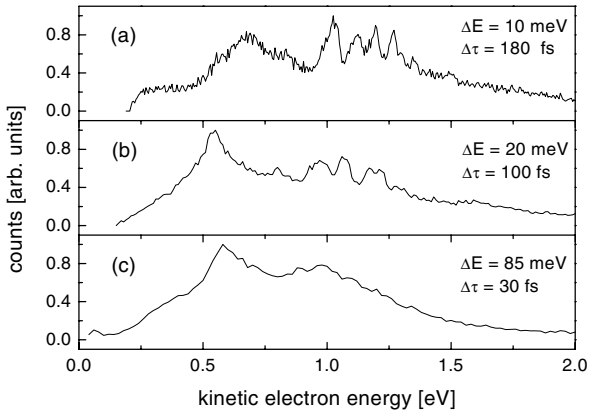

Fig. 5. Normalized photoelectron spectra in the low kinetic energy range up to 2 eV recorded for three different 800 nm laser pulse durations τ, respectively bandwidths ΔE at approximately 5×10^{12} W/cm^2.

the polarization but still reduced for perpendicular polarization. These electrons might partially originate from multiphoton ionization without intermediate Rydberg resonances. Further experiments on details of the angular distribution using imaging techniques are on the way.

As a final observation in this subsection we compare different pulse durations. Figure 5 shows normalized photoelectron spectra obtained with 800 nm radiation at approximately 5×10^{12} W/cm^2 for three laser setups with different Fourier limited pulse durations τ and corresponding bandwidths ΔE. The spectra — albeit broadened in accord with the bandwidth — indicate that the excitation mechanism must be very fast: traces of a Rydberg population can be observed even for pulses as short as 30 fs.

We can summarize here that for a realistic description of the excitation process of Rydberg series a full MAE/NMED picture is needed. In the course of this paper, particularly when presenting the results of the two-color pump-probe study in the following section and the comparison of the hot and cold fullerene response in Section 3.3 further convincing arguments for this statement will be given.

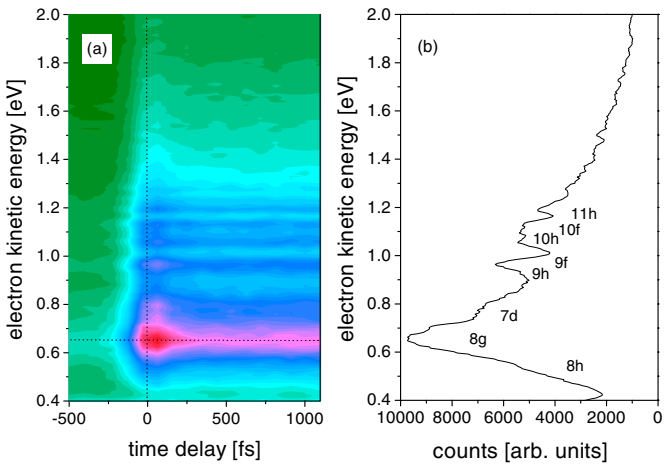

Fig. 6. (a) Contour plot of the photoelectron signal as a function of the time-delay between 400 nm pump (1×10^{11} W/cm^2) and 800 nm probe pulse (2×10^{12} W/cm^2). (b) Kinetic energy distribution of photoelectrons for zero time-delay, which corresponds to a vertical cut along the vertical dotted at zero time delay line shown in the left panel.

3.2 Two-color pump-probe spectroscopy

As discussed in the previous subsection the chirp dependence of the photoelectron spectra (Fig. 2) indicates that it might be possible to separate several steps of the excitation and detection process. Here we use a blue pump pulse of relatively low intensity, which is resonant with the dipole-allowed HOMO (h_u) $\rightarrow$ LUMO+1 (t_{1g}) transition (see Fig. 3, right diagram), to deposit energy more efficiently into the electronic system. The dynamics of the energy redistribution within the electronic system and the accompanied coupling to the nuclear motion is then probed by a time-delayed red probe pulse. We choose the polarization of the two pulses to be perpendicular, the red pulse pointing towards the detector. The enhancement of the photoemission yield along the polarization axis (Fig. 4) offers a simple way to discriminate "background" photoelectrons ionized with blue photons only from those originating from the red probe pulse.

The photoelectron spectra recorded as a function of the time-delay between 400 nm pump (1×10^{11} W/cm^2) and 800 nm probe-pulse (2×10^{12} W/cm^2) are shown by the contour plot in Figure 6a. The plot was obtained by interpolating the spectra measured at different time-delays with a total number of 2×10^6 laser shots in each step. Since good spectral and temporal resolution are mutually exclusive, 100 fs pulses with a bandwidth of $\Delta E = 20$ meV were used as a compromise in the two-color experiments. This allows the assignment of several excited Rydberg levels, though rather poorly resolved, as well as to monitor the dynamics. A cut through this contour plot for zero time-delay along the vertical dotted line is given in Figure 6b. It corresponds to a photoelectron spectrum which essentially reproduces the features obtained in the one color (800 nm) experiments (Fig. 3a) — except for a poorer spectral resolution due to the shorter pulses.

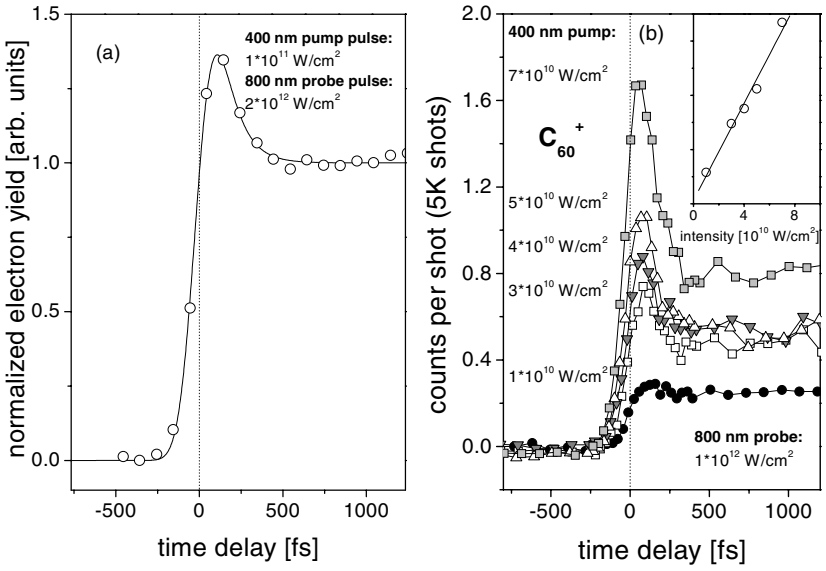

Fig. 7. (a) Normalized photoelectron yield upon excitation of the $8g$ Rydberg state as a function of the time-delay between blue pump and red probe pulse (open circles). Zero photoelectron yield has been set at the low intensity level for negative time-delays and $t = 0$ to the turning point of the error function. (b) Time evolution of the total C_{60}^+ ion yield depending on the pump pulse intensities with a linear intensity dependence of the maximum signal (inset). $t = 0$ was determined by measuring the cross correlation of xenon photoions (not shown).

Figure 6a shows that at negative time delay when the red pulse leads, almost no photoemission signal from excited Rydberg states is observed. Once pump and probe pulse overlap the photoelectron yield increases dramatically and a maximum population of the Rydberg series if found at a time delay of 50–100 fs. It can be inferred from this observation that the resonant pre-excitation of the LUMO+1 (t_{1g}) state by the weak blue laser pulse is essential to populate Rydberg states for such low energies of the red pulse (note that in contrast to Figure 6a where the red pulse fluence is only $0.2\,\mathrm{J/cm^2}$ the spectrum shown in Fig. 3a was recorded with a red pulse fluence of $1.65\,\mathrm{J/cm^2}$). The population of this state is clearly identified as the bottleneck in the excitation process. It acts as a "doorway state" to the population of Rydberg levels. At time delays longer than 400 fs the photoelectron spectra remain nearly the same for several picoseconds. In Figure 7a this is shown more quantitatively for the photoelectron yield from the $8g$ Rydberg state. The spectrum shown results from a horizontal cut through the contour plot along the t axis at an electron kinetic energy corresponding to the $8g$ Rydberg state.

The interpretation of the experimental data has benefited from recent theoretical work by Zhang et al. [4]. In these calculations the laser frequency is tuned to the first dipole allowed transition HOMO (h_u) $\rightarrow$ LUMO+1 (t_{1g}). Although, the pulse duration of 10 fs and the laser intensity of $3 \times 10^{10}\,\mathrm{W/cm^2}$ used in the calculation do not exactly match the experimental conditions of our time-resolved two-color experiment, some interesting general trends described in the theoretical work are highly pertinent to the present discussion. The calculation predicts that the initial electronic configuration of C_{60} especially the HOMO (h_u) and LUMO+1 (t_{1g}) is significantly changed upon laser irradiation. Even at these low intensities two electrons are excited to the LUMO+1 orbital during the laser pulse, while at the same time the energy position of the t_{1g} electronic state shifts downwards, and h_u shifts upwards. According to the calculation the energy shift results mainly from a reduction of the symmetry from I_h to D_{5d} (Jahn-Teller effect) which splits the degenerate h_u and t_{1g} into several energetically separated sublevels. Because of this symmetry reduction the C_{60} ionic core finds itself in a non-equilibrium position at the end of the laser excitation and starts to vibrate. The lattice and the electronic system exchange almost 2 eV with an oscillation period of about 84 fs. The authors attribute this to the excitation of the well-known $a_g(1)$ radial breathing mode [40]. Its vibrational period has been determined experimentally to be 67 fs [41]. Two more results of this theoretical work are worth mentioning here. First, the total absorbed energy slightly overshoots the energy deposited into C_{60} at the end of the laser pulse. The authors attribute this to the influence of the lattice vibrations on the absorption process. Second, in the intensity range of about $10^{11}\,\mathrm{W/cm^2}$ the number of excited electrons increases almost linearly with intensity.

Guided by these theoretical predictions, it is assumed that the time-dependent electron signal in the two-color experiment shown in Figure 7a results from the combined effect of the doorway state population due to multielectron excitation and an additional fast relaxing excitation channel indicated by the hump in the photoelectron yield. The fast relaxation is attributed tentatively to a thermalization of the multiple excited electrons in the LUMO+1 orbital. For further evaluation we used a fit function $f(t) = f_1(t)f_2(t)$. The first term describes the population of the excited state which is essentially the integration over the Gaussian pulse envelope: $f_1(t) \propto 1+\mathrm{erf}(t/t_1)$. We used $t_1 = 110$ fs which corresponds to the cross correlation function of the blue and the red pulse. The second term characterizes the relaxation: $f_2(t) \propto 1 + p_a \exp(-t/t_2)$. The best fit was achieved with a value of $t_2 = 95$ fs for the fast relaxation time within the electronic degrees of freedom (solid line in Fig. 7a). This value is comparable to the characteristic time for thermalization due to

electron-electron scattering below ca. 100 fs, previously concluded from single pulse experiments [7,9]. At lower blue intensity the hump disappears, indicating that less electrons are injected into the "excited state bands" [19]. The life time of the doorway state (after excitation by the 400 nm pulse) is surprisingly long (ps up to ns) and seems to depend on the exit channel monitored [19]. One has to bear in mind that the population of the doorway state is probed here via the population of the Rydberg states which are excited resonantly out of the electron distribution in the doorway state by three (possibly two) red photons. With the present time resolution, it is not possible to resolve the periodic exchange of energy between the excited electron cloud and the molecular vibrations predicted by theory [4]. However, the measured lifetime of the excited state is comparable to the time the $a_g(1)$ vibration persists, when impulsively excited in time-resolved transmittance experiments on thin C_{60} films [33]. Thus, it is reasonable to assume that in our pump-probe scheme the energy deposited indeed partially oscillates between the electronic and nuclear system.

The time-dependence observed in the electron spectra is also found in the time-evolution of the total C_{60}^+ ion yields in the mass spectra. This is shown in Figure 7b using different intensity laser pulses in the range of 1×10^{10} to 7×10^{10} W/cm^2 for the 400 nm pump pulse and a slightly different intensity of 1×10^{12} W/cm^2 for the 800 nm probe pulse. This result underlines the bottleneck character of the LUMO+1 state in the energy deposition process, i.e. the ionization dynamics of the molecule is mainly governed by the dynamics of the initial excitation step. Furthermore, the approximately linear increase of electron density in the t_{1g} electronic state with increasing pump intensity predicted by theory [4] is also reflected in the C_{60}^+ ion yields. This is shown in the inset of Figure 7b, where the maximum C_{60}^+ signal is plotted as a function of the pump pulse intensity. The scaling of the y-axis is identical to that in the time resolved measurements.

The main excitation steps of the two-color pump probe experiments are illustrated in the orbital energy diagram of the C_{60} in Figure 8, which has been used already in the context of the wavelength dependent studies (see Sect. 3.1). Two additional pieces of information are derived exclusively from the pump probe study: (i) the resonantly pre-excited LUMO+1 state is the bottleneck to the Rydberg state manifold. This is indicated by the circles in Figure 8. (ii) The doorway state (and consequently the periodic exchange of 1 eV per excited electron with vibrational modes) indicated by the double arrows persists for several ps up to ns. The coupling to the nuclear motion plays a key role in the population of the Rydberg manifold. These are collective many particle effects providing a broad energy bandwidth, from which all the observed Rydberg states are accessible by the absorption of 2–3 photons. In a last one-photon step the Rydberg states are subsequently ionized into the continuum as illustrated for different scenarios (a–c) in Figure 8.

Some information on the "average" order of the multiphoton processes can be obtained by investigation of the

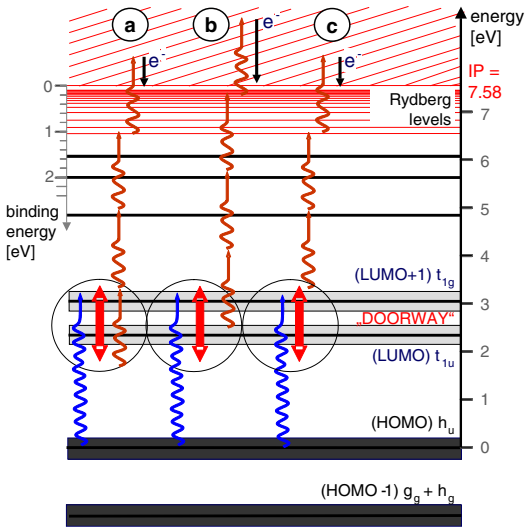

Fig. 8. Schematic orbital energy level diagram of C_{60} as already described in the context of the wavelength dependent studies (Fig. 3). Different excitation processes of Rydberg levels (a–c) involving 2–3 photons plus one additional photon for ionization into the continuum are indicated.

C_{60}^+ ion yield depending on the red probe pulse intensity. This analysis has to be taken with a grain of salt since in contrast to a genuine multiphoton process, where n photons are taken simultaneously from the laser field, in order to promote *one* electron (SAE) into the continuum, in case of C_{60} *many* electrons (MAE) are excited — possibly in the same set of unoccupied orbitals. We recall that in lowest-order perturbation theory the n-photon ionization rate Γ_n from a bound to a free (continuum) state is given by $\Gamma_n = \sigma_n I^n$, where n is the minimum number of photons needed for ionization, σ_n is the generalized cross section and I is the incident laser intensity. According to this equation, the C_{60}^+ signal should follow in a double logarithmic diagram a straight line with the slope n when increasing the intensity I of the red probe pulse. The order of the process should be lower compared to direct multiphoton ionization due to the pre-excited LUMO+1 doorway state. In Figure 9a, the ion signal is evaluated in the "plateau region" of the time dependent measurements displayed in Figure 9b. Already the blue excitation pulse only with its 3×10^{11} W/cm^2 causes some ionization, which is indicated by the horizontal line. The ionization rate of pre-excited molecules increases significantly above a threshold probe pulse intensity of $I_t = 1.1 \times 10^{12}$ W/cm^2 with a slope of $n = 2.75$. The threshold intensity is defined as the intersection of the linear fit with the blue only signal (horizontal line). At highest probe pulse intensities used in these experiments (3×10^{12} W/cm^2) the C_{60}^+ ion yield starts to saturate. To guide the eye, the intensity dependence of the ionization rate on the red probe pulse intensity is indicated by the dotted curve. At first sight, the slope of n = 2–3 is quite surprising. One would expect to need 3–4 red photons for the ionization from the excited doorway state as indicated in the orbital energy diagram of Figure 8, especially after some energy is flown

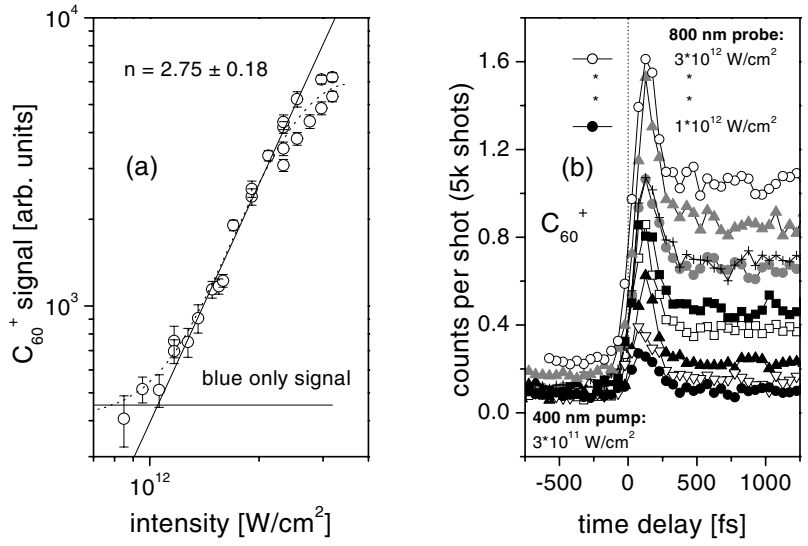

Fig. 9. (a) Double-logarithmic plot of the C_{60}^{+} ion signal evaluated in the "plateau" region (time delay > 500 fs in the right panel) as a function of the red probe pulse intensity. Also indicated in the Figure are the ion signal resulting from irradiation with blue pump pulses only (horizontal line) and the slope ($n = 2.75$) of its increase due to red probe pulses of increasing intensity. For details, see the text. (b) Time evolution of the total C_{60}^{+} ion yield depending on the probe pulse intensities. A cross-correlation measurement of xenon ions (not shown) gives $t = 0$.

into nuclear vibrations. On the other hand, the power law is only valid if no resonances are hit during the multiphoton excitation. In the excitation process we discuss here the Rydberg states as intermediate resonances towards the ionization which may be the cause for the observed slope of 2–3. However, we cannot rule out with certainty that the ionisation process might be of statistical nature. This would also lead to slopes in the log-log plot, which corresponds to the minimum number of photons needed for ionisation [9].

So far, non-adiabatic multielectron effects have been discussed solely with respect to the excitation of Rydberg states and their subsequent single-photon ionization. We have experimental evidence that these mechanisms are also active in, both multiple ionization at higher intensities and fragmentation processes of the molecule. Again, mass spectra have been recorded as a function of the time-delay between a 400 nm pump and a 800 nm probe pulse. However, in order to create a sufficient amount of doubly charged ions and fragments we have used in these experiments an intensity of $7 \times 10^{12}\,\mathrm{W/cm^2}$ for the blue pulse — which is about 2 orders of magnitude higher than in the previously discussed experiments. The red probe pulse was $4 \times 10^{12}\,\mathrm{W/cm^2}$ only slightly more intense than previously. In Figure 10, the time-dependent total ion yields of doubly charged fragments (open circles), doubly charged mother ions (solid circles), singly charged fragments (open triangles), and singly charged mother ions (solid triangles) are shown. Since already the pump pulse causes significant ionization and fragmentation, the total ion yields are normalized to the sum of the single-pulse ion yields for both wavelength. A cross-correlation measurement using the xenon ion signal gives $t = 0$ and $\tau = 125 \pm 5$ fs. The comparison of negative and positive time-delays with respect to the ion yields shows that multielectron excitation to the LUMO+1 doorway state by the blue pulse increases the signal of doubly charged mother ions and doubly charged fragments significantly. The characteristic hump 50–100 fs after zero time-delay indicates that fast thermalization within the hot electron cloud in combination with coupling

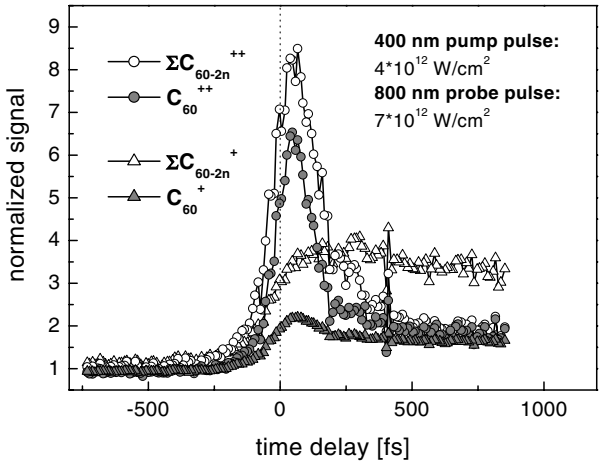

Fig. 10. Total ion yield of $\sum C_{60-2n}^{++}$ (open circles), C_{60}^{++} (solid circles), $\sum C_{60-2n}^{+}$ (open triangles), and C_{60}^{+} (solid triangles) as a function of the time-delay between 400 nm pump ($4 \times 10^{12}\,\mathrm{W/cm^2}$) and 800 nm probe pulse ($7 \times 10^{12}\,\mathrm{W/cm^2}$). The total ion yields are normalized to the sum of the single-pulse ion yields for blue and red pulses. $t = 0$ have been determined by a cross-correlation measurement of xenon. Its width was $\tau = 125 \pm 5$ fs.

of the electronically excited state to molecular vibrations determine not only the population of Rydberg levels, but also the rate constant for multiple ionization through a very efficient energy absorption. It shows that multiple ionization occurs predominantly sequentially, which has been concluded previously from single-pulse experiments [9,42]. Regarding the subsequent fragmentation into singly and doubly charged species, different processes seem to be involved. The ion yield of doubly charged fragments follows both, the multielectron excitation dynamics of the doorway state (heating of the electron and nuclear system) and the yield of doubly charged mother ions. This indicates that doubly charged fragments result predominantly from hot C_{60}^{++} ions, which are formed and excited during

the interaction, for instance by internal energy conversion, by shake processes in the ionic system [43] or even (albeit certainly to a lesser extent only) by recollision processes with emitted electrons within one laser oscillation cycle [44]. In contrast, the formation of singly charged fragments does not exhibit such a pronounced time dependent behavior. The pre-excitation of the doorway state with the blue pump pulse followed by vibrational coupling significantly enhances fragmentation, but the characteristic "hump" in the time-dependent signal 50–100 fs after time zero is missing for these (blue) pump laser pulse intensities. As intuitively expected, the "overheated" electron cloud in the doorway state enhances multiple ionization of C_{60} resulting in multiply ionized fragments as described above, rather than the formation of single charged fragments. The electron phonon-coupling time is on the order of a few hundred fs [9], much longer than the time the hot electron cloud persists. A detailed discussion of photoinduced fragmentation dynamics in C_{60} fullerenes studied with fs pump-probe spectroscopy will be subject to future work [45].

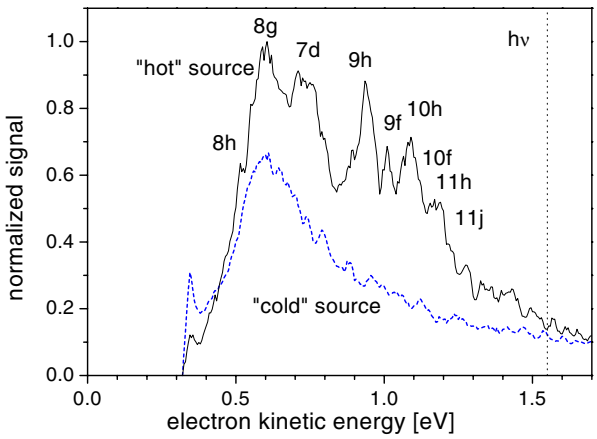

Fig. 11. Comparison of the photoelectron signal as a function of kinetic energy from "hot" (770 K, solid line) and "cold" C_{60} (80 K, dashed line) [19]. 800 nm pulses of 100 fs length (2.5×10^{12} W/cm^2) were used for Rydberg excitation and detection. The two curves are normalized to each other at an electron energy of 2 eV where only a thermal electron distribution is detected.

3.3 Hot and cold C_{60}

At this point one is tempted to question again the role of initial vibrational excitation of the C_{60}. Although that energy cannot be accessed in a direct multiphoton excitation or ionization process as discussed above, energy exchange between electronic and vibrational system may significantly profit from the thermal energy stored in the system. In view of the excitation process of Rydberg series, a change of the excited state geometry will change the Franck-Condon region for subsequent excitation of the Rydberg levels, thus giving access to at least some of the vibrational energy content. Hence, experiments have been performed comparing "hot" (770 K) and "cold" (80 K) C_{60} target molecules [19], in order to control the strength of vibrational coupling in the excitation process and to study its effect on the systems response to ultrashort, intense laser pulses.

In the "hot" C_{60} about 23% and 8% of the molecules are in the vibrationally excited $v = 1$ and $v = 2$ states of the $h_g(1)$ mode, respectively, while at 80 K the molecule is predominantly in its vibrational ground state with the population of the lowest vibrationally excited state being as low as 0.6%. The data have been taken in a one color experiment with a single pulse of 800 nm photons, 100 fs duration and an intensity of 2.5×10^{12} W/cm^2. The result is shown in Figure 11. The photoelectron spectra recorded for hot fullerenes exhibit the rich structure of Rydberg states discussed in previous sections. In contrast, the structure has completely disappeared in the photoelectron spectrum from cold C_{60}. Following the above discussion this can be understood in terms of the much higher population of vibrationally excited states for the hot molecule which increases the effective density of populated rovibrational states and consequently enhances electron-phonon coupling. Note also that multielectron dynamics in the excited doorway state — as initiated by the strong laser field — involves already per se a band of excited states filled with hot electrons which can couple to the nuclear bath the more efficiently the more it is pre-excited[1]. In summary, the NMED process leads to an efficient population of a relatively broad energy band in case of hot C_{60}. This broadening is essential for accessing the manifold of excited Rydberg states due to the absorption of several additional photons. For cold C_{60} the energy distribution of photoelectron emission follows essentially the statistical "thermal" electron energy distribution — a behavior which lends itself to the interpretation that electron-phonon coupling is much weaker when the system is cold. Similar effects have been observed, for instance, in 2-photon photoelectron spectroscopy on silver surfaces [46].

4 Conclusion

The energetics and dynamics of the ultrafast response of C_{60} fullerenes to intense short pulse radiation has been investigated with photoelectron and photoion spectroscopy. In order to obtain a detailed understanding, especially of the population mechanism of Rydberg states upon laser irradiation of the neutral molecule, single-pulse and two-color femtosecond pump probe experiments were performed. By studying the effect of different laser parameters such as excitation wavelength, intensity, chirp, and polarization in single-pulse experiments and the time

[1] In a SAE picture one would possibly speak about more efficient internal conversion at conical intersections due to a higher density of states in the energetically accessible region. This in turn would significantly change the Franck-Condon region so that the vibrational propensity rule discussed earlier is relaxed and nuclear energy may be transferred.

and intensity dependence in two-color pump-probe experiments new insights into the underlying processes are obtained.

The experimental results point towards an excitation process including four main steps: (i) at the beginning of the laser pulse nonadiabatic multielectron excitation from the HOMO (h_u) leads to a very efficient population of the LUMO+1 (t_{1g}), which is considered to be the doorway state for all subsequent processes. (ii) The rapid thermalization within the electronic system on a time scale below 100 fs and the coupling of the electronic excitation to nuclear motion of the molecule results in a the population of a broad energy band of 1–2 eV depending on the photon energy. The energy is stored for at least several picoseconds in the doorway state without discernable relaxation. (iii) The "level broadening" allows the population of Rydberg states via multiphoton absorption, as well as excitation of some lower-lying levels. (iv) This is followed by single photon ionization from the excited states resulting in a characteristic sequence of photoelectron peaks.

Investigation of cold C_{60} molecular beams with reduced vibrational energy content and hence, reduced phonon density highlight the importance of electron-phonon coupling in the excitation process of Rydberg states. Due to the reduced vibrational coupling, the characteristic signature of populated Rydberg levels in the photoelectron spectra is absent.

As shown by TDDFT calculations the singe active electron picture — although it may describe some observations for low intensity and particularly short pulses rather nicely — is not sufficient to describe the details of the electronic response. If the nuclear degrees of freedom come into play — which is obviously the case for Rydberg excitation as shown by comparing hot and cold target molecules — one needs to study the full picture, involving all couplings and degrees of freedom.

The comparison of the experimental results with recent theoretical work gives a strong indication that nonadiabatic multielectron dynamics (NMED) plays a key role for the understanding of the response of C_{60} to short-pulse laser radiation. Time-resolved photoion spectroscopy at higher laser intensities show that these mechanisms are also active in multiple ionization and fragmentation of the molecule. In this context, a rigorous theoretical treatment would be highly desirable combining the relevant approaches presently discussed — such as NMED and time dependent potential surfaces, field induced crossings splitting into one uniform, rigorous approach.

It is evident that a detailed understanding of a system, such as a fullerene, helps to understand the physics of a whole class of molecules and clusters with an extended π electron system exposed to intense laser light. It will also help to model control schemes of certain relaxation pathways in large finite molecular system.

We thank Professor T.F. George (University of Missouri-St.Louis) and Professor G.P. Zhang (Indiana State University) for very helpful discussions. Financial support from Deutsche Forschungsgemeinschaft through Sonderforschungsbereich 450, the Access to Research Infrastructures activity in the Fifth Framework Program of the EU (HPRI-CT-1999-00084), the EU IHP "Cluster Cooling" Network and Vetenskapsrådet is gratefully acknowledged.

References

1. A.D. Bandrauk, R.J. Gordon, Y. Fujimura, *Laser Control and Manipulation of Molecules* (Oxford University Press, Oxford, 2002)
2. R.J. Levis, G.M. Menkir, H. Rabitz, Science **292**, 709 (2001)
3. B. Torralva, T.A. Niehaus, M. Elstner, S. Suhai, T. Frauenheim, R.E. Allen, Phys. Rev. B **64**, 153105 (2001)
4. G.P. Zhang, X. Sun, T.F. George, Phys. Rev. B **68**, 165410 (2003)
5. E.E.B. Campbell, G. Ulmer, I.V. Hertel, Phys. Rev. Lett. **67**, 1986 (1991)
6. F. Rohmund, M. Heden, A.V. Bulgakov, E.E.B. Campbell, J. Chem. Phys. **115**, 3068 (2001)
7. E.E.B. Campbell, K. Hansen, K. Hoffmann, G. Korn, M. Tchaplyguine, M. Wittmann, I.V. Hertel, Phys. Rev. Lett. **84**, 2128 (2000)
8. I.V. Hertel, T. Laarmann, and C. P. Schulz, in *Advances in Atomic, Molecular, and Optical Physics*, edited by B. Bederson, H. Walter (Elsevier Academic Press, San Diego, 2005), Vol. 50, pp. 219–286
9. K. Hansen, K. Hoffmann, E.E.B. Campbell, J. Chem. Phys. **119**, 2513 (2003)
10. M. Tchaplyguine, K. Hoffmann, O. Dühr, H. Hohmann, G. Korn, H. Rottke, M. Wittmann, I.V. Hertel, E.E.B. Campbell, J. Chem. Phys. **112**, 2781 (2000)
11. P. Agostini, F. Fabre, G. Mainfray, G. Petite, N.K. Rahman, Phys. Rev. Lett. **42**, 1127 (1979)
12. M. Boyle, K. Hoffmann, C.P. Schulz, I.V. Hertel, R.D. Levine, E.E.B. Campbell, Phys. Rev. Lett. **87**, 273401 (2001)
13. M.J. Puska, R.M. Nieminen, Phys. Rev. A **47**, 1181 (1993)
14. L.V. Keldysh, Sov. Phys. JETP **20**, 1307 (1965).
15. A.M. Perelomov, V.S. Popov, M.V. Terentev, Sov. Phys. JETP **23**, 924 (1966)
16. M.V. Ammosov, N.B. Delone, V.P. Krainov, Sov. Phys. JETP **64**, 1191 (1986)
17. M. Lezius, V. Blanchet, D. M. Rayner, D.M. Villeneuve, A. Stolow, M.Y. Ivanov, Phys. Rev. Lett. **86**, 51 (2001)
18. M. Lezius, V. Blanchet, M.Y. Ivanov, A. Stolow, J. Chem. Phys. **117**, 1575 (2002)
19. M. Boyle, M. Hedén, C.P. Schulz, E.E.B. Campbell, I.V. Hertel, Phys. Rev. A **70**, 051201 (2004)
20. K. Hansen, R. Müller, P. Brockhaus, E.E.B. Campbell, I.V. Hertel, Z. Phys. D **42**, 153 (1997)
21. V. Schyja, T. Lang, H. Helm, Phys. Rev. A **57**, 3692 (1998)
22. S. Larochelle, A. Talebpour, S.L. Chin, J. Phys. B **31**, 1201 (1998)
23. M.S. Dresselhaus, G. Dresselhaus, P.C. Eklund, *Science of Fullerenes and Carbon Nanotubes* (Academic Press, San Diego, 1996)
24. R.R. Freeman, P.H. Bucksbaum, H. Milchberg, S. Darack, D. Schumacher, M.E. Geusic, Phys. Rev. Lett. **59**, 1092 (1987)
25. I.V. Hertel, H. Steger, J. De Vries, B. Weisser, C. Menzel, B. Kamke, W. Kamke, Phys. Rev. Lett. **68**, 784 (1992)

26. F. Remacle, R.D. Levine, J. Phys. Chem. A **105**, 2708 (2001)
27. A.N. Markevitch, S.M. Smith, D.A. Romanov, H.B. Schlegel, M.Y. Ivanov, R.J. Levis, Phys. Rev. A **68**, 011402 (2003)
28. A.N. Markevitch, D.A. Romanov, S.M. Smith, H.B. Schlegel, M.Y. Ivanov, R.J. Levis, Phys. Rev. A **69**, 013401 (2004)
29. H. Kono, Y. Sato, Y. Fujimura, I. Kawata, Laser Physics **13**, 883 (2003)
30. H. Kono, Y. Sato, N. Tanaka, T. Kato, K. Nakai, S. Koseki, Y. Fujimura, Chem. Phys. **304**, 203 (2004)
31. C.P. Schick, P.M. Weber, J. Phys. Chem. A **105**, 3725 (2001)
32. N. Kuthirummal, P.M. Weber, Chem. Phys. Lett. **378**, 647 (2003)
33. S. Dexheimer, D. Mittleman, R. Schoenlein, W. Vareka, X.-D. Xiang, A. Zettl, C. Shank, in *Ultrafast Phenomena VIII*, Vol. 55 of Springer Series in Chemical Physics, edited by J.-L. Martin, A. Migus, G. Mourou, A. Zewail (Springer, Berlin, Heidelberg, 1993), pp. 81–82
34. S.B. Fleischer, B. Pevzner, D.J. Dougherty, H.J. Zeiger, G. Dresselhaus, M.S. Dresselhaus, E.P. Ippen, A.F. Hebard, Appl. Phys. Lett. **71**, 2734 (1997)
35. V.R. Bhardwaj, P.B. Corkum, D.M. Rayner, Phys. Rev. Lett. **91**, 203004 (2003)
36. T. Kunert, R. Schmidt, Phys. Rev. Lett. **86**, 5258 (2001)
37. T. Kunert, R. Schmidt, `http://www.dymol.org/c60.html`
38. G.P. Zhang, T.F. George, Phys. Rev. Lett. **93**, 147401 (2004)
39. D. Bauer, F. Ceccherini, A. Macchi, F. Cornolti, Phys. Rev. A **64**, 063203 (2001)
40. J. Menndez, J.B. Page, in *Light Scattering in Solids*, edited by M. Cardona, G. Güntherodt (Springer, Heidelberg, 2000), Vol. VIII
41. Z.H. Dong, P. Zhou, J.M. Holden, P.C. Eklund, M.S. Dresselhaus, G. Dresselhaus, Phys. Rev. B **48**, 2862 (1993)
42. E.E.B. Campbell, K. Hoffmann, H. Rottke, I.V. Hertel, J. Chem. Phys. **114**, 1716 (2001)
43. A. Reinköster, S. Korica, G. Prumper, J. Viefhaus, K. Godehusen, O. Schwarzkopf, M. Mast, U. Becker, J. Phys. B **37**, 2135 (2004)
44. V.R. Bhardwaj, P.B. Corkum, D.M. Rayner, Phys. Rev. Lett. **93**, 043001 (2004)
45. M. Boyle, T. Laarmann, I. Shchatsinin, C.P. Schulz, I.V. Hertel, J. Chem. Phys. **122**, 181103 (2005)
46. E. Knoesel, A. Hotzel, T. Hertel, M. Wolf, G. Ertl, Surf. Sci. **368**, 76 (1996)